



Numerically evaluating energetic composite flame propagation with thermally conductive, high aspect ratio fillers

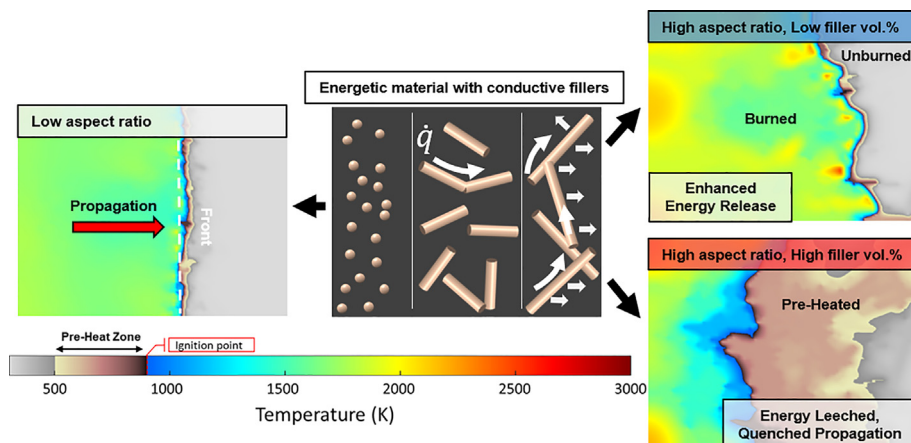
Miles C. Rehwoldt^{a,b,1}, Dylan J. Kline^{a,b,1}, Michael R. Zachariah^{a,*}

^a University of California, Riverside, CA 92521, USA

^b University of Maryland, College Park, MD 20740, USA



GRAPHICAL ABSTRACT



ARTICLE INFO

Article history:

Received 19 May 2020

Received in revised form 18 August 2020

Accepted 26 August 2020

Available online 31 August 2020

Keywords:

Polymer-matrix composites

Thermal properties

Heat transfer

Material modeling

Energetic materials

ABSTRACT

Thermally conductive, high aspect ratio additives offer a way to modulate heat transfer for flame propagation of energetic materials by creating “highways” along which released energy can transfer to unreacted regions. Flame propagation in dense energetic composites filled with randomly orientated additives of varied filler volume percentage (vol%), aspect ratio (AR), and thermal conductivity was modeled using a 2D implicit finite element method. It was found that small additions (<20 vol%) of high thermal conductivity, high aspect ratio additives (AR > 25) enhanced the total area burned by as much as ~25% and the energy released by as much as ~10%. While lower aspect ratio additives (AR < 25) resulted in negligible enhancements due to the lack of thermally conductive pathways, large amounts of additives (>20 vol%) oftentimes led to quenched flame propagation by excessive leeching of energy from the reaction front. This study serves as a proof-of-concept to enhance energy release by increasing heat transfer with additives that can be incorporated into energetic composites.

© 2020 Published by Elsevier Ltd.

1. Introduction

Advanced energetic and propellant systems are increasingly being viewed as good candidates for additive manufacturing. This is particularly so when considering the use of nanomaterials which

* Corresponding author.

E-mail address: mrz@engr.ucr.edu (M.R. Zachariah).

¹ Co-First Author.

make traditional casting difficult. These systems rely on high volume loadings of a sub-micron metal fuel and an oxidizer either in the form of a polymer binder or sub-micron source of condensed oxygen (e.g. metal oxides, ammonium perchlorate). For full utility, these materials must not only have high energy density, but must release its chemically stored energy in a rapid, stable manner and must be mechanically durable. One significant aspect of the operational characteristics of self-sustained combustion in these materials is heat feedback to maintain flame front propagation, which implies that thermal transport properties play an important role. These materials fall into a much broader class of polymer composites.

Characterizing the tunability of thermal and mechanical properties of multi-phase (Cheng and Vachon, 1969) polymer systems has been difficult to explore both experimentally (Maiti and Ghosh, 1994; Kargar et al., 2018; Yuan et al., 2017; Smith et al., 2017) and theoretically (Pal, 2008; Pietrak and Wiśniewski, 2015; Nielsen, 1974) despite its importance in a variety of applications which include energy storage for electronics (Yuan et al., 2017; Dang et al., 2013), electrical shielding (Maiti and Ghosh, 1994; Wanasinghe et al., 2020), and heat exchange technologies (Maiti and Ghosh, 1994; Yuan et al., 2017; Du et al., 2018). Commonly used epoxies, acrylates, and fluoropolymers are poor conductors of heat and are generally treated as thermal insulators (Lawless et al., 2020). Thermally conductive fillers like carbides (Yuan et al., 2017), metals (Maiti and Ghosh, 1994; Meeks et al., 2017), and carbon structures (Kargar et al., 2018; Du et al., 2018; Agarwal et al., 2008; Zheng et al., 2012) with various morphologies (i.e. fibers, spheres, flakes) are oftentimes utilized to modulate the composite's effective thermal conductivity. General candidate materials span a wide range of thermal conductivities as can be seen in Fig. 1. Improvements to thermal conductivity in composites has been primarily observed with the addition of thermally conductive fillers such as silver particles (Maiti and Ghosh, 1994), graphite (Zheng et al., 2012), carbon fibers (Agarwal et al., 2008), and carbon nanotubes (Smith et al., 2017; Du et al., 2018) (CNTs).

Despite the widespread experimental and theoretical work studying the effects of thermally conductive materials on the effective thermal conductivity of two-phase polymer systems, little modeling work has investigated the extent to which the inclusion of such materials effects flame propagation performance in self-propagating high temperature synthesis (SHS) (Mukasyan and Shuck, 2017; Rogachev and Baras, 2007; Song et al., 2011) and propellant systems (Cheng and Vachon, 1969; Smith et al., 2017; Meeks et al., 2017; Isert et al., 2017). Systems of primary interest are those which imbed condensed phase energetic constituents in the form of micron to nanoscale metal fuels, oxidizers, and/or other applicational additives of various morphologies within a polymer matrix binder (Rehwoldt et al., 2020; Kline et al., 2020; Yan et al., 2012; Chen et al., 2012; McClain et al., 2019; Wang et al., 2018; An et al., 2019; Shen et al., 2020; Huang et al., 2014; Muravyev et al., 2019).

In this paper, we explore the inclusion of materials with high thermal conductivity as a means to augment the energy release rate in a dense composite (Goroshin et al., 1998). In the absence of convective heat transfer, flame propagation behavior is dependent on how fast energy can be generated (chemistry) and how fast that released energy can be transferred to unreacted areas (thermal diffusivity). Thus, for a composite material with constituents having roughly the same order of magnitude of the specific thermal mass ($\sim 10^6 \text{ J m}^{-3} \text{ K}^{-1}$), ρc_p , the local flame behavior is explicitly a function of the local thermal conductivity (Turns, 2012). The role of filler material parameters (e.g. volume percentage, material type, and geometric morphology) on composite properties have been explored with experimental studies which reference effective

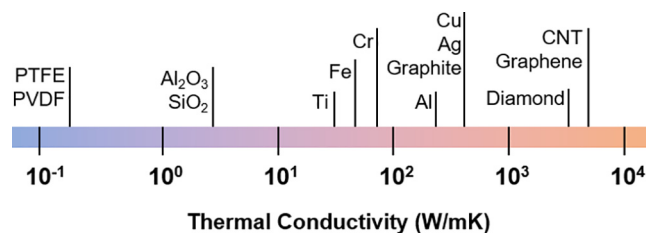


Fig. 1. Spectrum of thermal conductivities typically used in polymer composites with tunable thermal properties.

composite thermal conductivity theories, such as the Lewis-Nielson, Maxwell, and Percolation models (Maiti and Ghosh, 1994; Kargar et al., 2018; Pal, 2008; Pietrak and Wiśniewski, 2015; Nielsen, 1974). Experiments and Lewis-Nielson models have shown that the use of rods or fibers results in superior effective composite thermal conductivity over sphere-like morphologies at similar volume fractions since high aspect ratio additives tend to easily form a connective network along directions of interest (Smith et al., 2017; Nielsen, 1974; Du et al., 2018; Agarwal et al., 2008).

Here, a 2D implicit finite difference numerical model of the heat equation is used to analyze flame propagation behavior of energetic systems with low thermal conductivity (e.g. Al/PVDF) which incorporate thermally conductive fillers of varied volume percentages (vol%), aspect ratios (AR), and thermal conductivity. More specifically, we focus on a cross sectional area parallel to flame propagation in which rods of random azimuthal orientation lay in the plane. Results illuminate how thermal properties and materials distribution within the energetic composite correlates to flame front morphology, permeability of heat, rate of material consumption, and changes to overall energy release.

2. Modeling structure

2.1. Thermal transport and chemistry

Self-sustaining combustion of a dense reactive material involves heat transfer initiating rapid chemistry, which in turn drives more heat transfer (Turns, 2012). The energy that is liberated during an exothermic reaction is converted to heat and observed as regions of temperature accumulation. Thermal gradients drive conductive energy transport from regions of high temperature to regions of low temperature through conductive pathways. For global flame propagation of a heterogenous reactive material to be self-sustaining, the combination of energy generated by chemistry and inward heat diffusion in local regions must equal or exceed outward heat diffusion in order to sustain the global reaction front (Turns, 2012). Rapid heat transfer from adjacent reacted materials ensures a rapid accumulation of energy to stimulate further chemical reactions. Often, the primary limitation to the observed propagation rate is that chemistry is so fast that the process is limited by the transport of heat to the unreacted region.

Under these conditions, the governing dynamics is described by the 2D Heat Equation (Equation (1)) in which only Fourier conductive heat transfer flux, $\vec{q}_{cond} = -k\vec{\nabla}T$, between discrete material regimes is considered with the assumption that the thermal conductivity is constant along conduction boundaries. Additionally, external volumetric heat input, P , and internal chemical energy generation, Q , need to be considered. We will discuss how the chemical generation term will be handled in a later section.

$$\rho c_p \frac{dT}{dt} = \frac{\partial}{\partial x} \left(k \frac{\partial T}{\partial x} \right) + \frac{\partial}{\partial y} \left(k \frac{\partial T}{\partial y} \right) + (P + Q) \quad (1)$$

It is assumed that material density is sufficiently large for mass diffusivity to be negligible compared to thermal diffusivity ($Le \ll 1$) so that mass diffusivity and convective behavior may be ignored (Varma et al., 2001; Bacciochini et al., 2013). The effective local thermal conductivity at the boundaries of discrete material regimes is determined by estimating thermal resistance (Equation (2)) (Cheng and Vachon, 1969; Pietrak and Wiśniewski, 2015; Varma et al., 2001; Ervin et al., 1999).

$$k_{\text{eff}} = \frac{2k_1k_2}{k_1 + k_2}, k_{p,q+\frac{1}{2}}^n = \frac{2k_{p,q+1}^n k_{p,q}^n}{k_{p,q+1}^n + k_{p,q}^n} \quad (2)$$

The specifics of discretization and numerical methods and solutions to the 2D Heat Equation are described in the supporting document.

The initial volumetric power input, P , (e.g. hot wire, laser, electrical) heats the material to the pre-defined ignition temperature, T_{ig} , and initiates volumetric chemical energy generation, Q . Since our intent is to focus on the role of heat transfer media, we simplify the chemistry as the product of the global specific reaction enthalpy of the energetic material, Δh_{rxn} , with the global conversion rate of the of the reactant material, $\frac{\partial \eta}{\partial t}$, which is proportional to the local concentration of reactant species (Merzhanov, 1969; Mukasyan and Rogachev, 2008; Beck and Volpert, 2003; Smolyakov, 2001).

Several assumptions of chemistry are made to simplify the model while maintaining the integrity of analyzed trends:

- Chemical reaction time scale is much shorter than that of diffusion ($t_{\text{rxn}} \ll t_{\text{diff}}$) (Beck and Volpert, 2003; Chakraborty and Swaminathan, 2007; Oberlack et al., 2000; Rogachev, 2003).
- Chemical kinetics is linearized with the assumption of a sufficiently large activation energy for the onset of chemical energy output at T_{ig} (Heaviside Function) (Rogachev and Baras, 2007; Varma et al., 2001; Mukasyan and Rogachev, 2008; Beck and Volpert, 2003).
- The adiabatic flame temperature, T_{ad} , serves as a surrogate for both the reaction enthalpy and the termination point of chemical energy generation (Heaviside Function).

Transient chemical energy generation is thus represented in Equation (3) in an implicit binary manner as a function of experimentally and theoretically determined temperature values ($T_{\text{ig}}, T_{\text{ad}}$) without the need for chemical conversion tracking.

$$Q = \Delta h_{\text{rxn}} \frac{\partial \eta}{\partial t} \rho c_p \approx \frac{T_{\text{ad}} - T_{\text{ig}}}{t_{\text{rxn}}} H(T - T_{\text{ig}}) H(T_{\text{ad}} - T) H(t_{\text{rxn}} - t_{\text{ig}}) \quad (3)$$

2.2. Physical layout

The physical platform of this model emulates that of the studies done by Varma et al. (2001), Grinchuk (2013), and Tang et al. (2009) in terms of geometry and discrete composition layout (Fig. S1). In accordance with a finite difference method, a constant volume (Tang et al., 2009) 2D mesh grid in a constant pressure environment is established with each grid point representing a temperature node at the center of a square area which has a characteristic width, δ (Becker and Kaus, 2016; Niragire, 2013). The grid represents an $L_y \times L_x$ frame with $\frac{L}{\delta}$ nodes along a single primary axis (grid resolution). Given the symmetry of the grid, one may choose to use the dimensionless length, $\chi_c = \frac{x}{\delta}$, where $\delta < L$.

The material properties of each node area represent a reactive material sample which is below or equal to its theoretical maximum density. This material properties may be varied to reflect the effects of composition morphology within the characteristic length. Each node area represents a composite of perfectly mixed

implicit solid constituents which are no larger than the characteristic length. Applicable systems of this model must be constrained by the following assumptions:

- The scales of primary particle heterogeneity within the energetic composite is smaller than the characteristic length (Fig. 2c).
- The thickness of the flame front is larger than the particle size and/or particle interspacing so that local flame propagation is treated as approximately quasi-homogenous (Goroshin et al., 1998; Varma et al., 2001; Beck and Volpert, 2003; Tang et al., 2009; Hwang et al., 1998; Mukasyan et al., 1999).

With these assumptions, specific geometric distribution of constituents within each square cell, δ^2 , can be ignored and one can simply use bulk quantities. One may effectively vary the magnification of a system to different length scales while maintaining the relative resolution of the grid (at the potential cost of solution accuracy). Each temperature node consists of an effective bulk thermal conductivity, k , specific heat, c_p , and local density, ρ . A two-phase mixture (Cheng and Vachon, 1969) is implemented by designating each node to be either energetic material or inert filler. This allows for a single effective thermal diffusivity value, α , to represent a single node of filler material, α_f , or energetic material, α_r . The filler material is a non-reactive material meant to simulate the physical existence of a material pore, longer range ($>\delta$) heterogeneity, a conductive additive, or any other relatively non-reacting niche filler. A mapping of discrete thermal diffusivities/conductivities of each grid point is generated as a visual for material distribution, as shown in Fig. 2.

The placement of filler material is randomized by house-built routines which aim to match the desired volume fraction of evenly distributed filler for a given calculation. Fig. 2b represents fillers with a non-spherical morphology in the form of rods whose centers of mass are uniformly distributed. The aspect ratio of the additive (AR) is monodisperse and varied between calculations. However, the minimum geometries of the rods are constrained by the model to be no smaller than the characteristic length. As the aspect ratio of the sample approaches unity (AR = 1), the distribution resembles the simple homogeneously mixed case shown in Fig. 2a. As discussed above, a primary assumption is that the length scale of the energetic composite's components is much smaller than the resolution of the grid, therefore the energetic material appears to be perfectly mixed (Fig. 2c).

2.3. Model analysis and parameters

The objective of this model is not to calculate specific numbers, but rather to flush out general trends for flame propagation behavior as a function of thermal properties, volume fraction of constituents, and the aspect ratio of incorporated rods. Although this model does not consider a specific system, many of the parameters for experimental conditions and thermophysical properties reflect those that would be seen in typical studies on fluoropolymer-bound energetic composites.

Modeling of flame behavior is assessed with room temperature initial conditions ($T_a = 300$ K) using $\frac{L}{\delta} = 100$ (e.g. $\delta = 2$ μm , $L = 200$ μm). Boundary conditions are set to allow for convective heat flux, $\dot{q}_{\text{conv}} = h(T - T_a)$, between the material and environment. The nonlinearity of radiative heat transfer disqualifies its contribution in this model which utilizes linear algebraic methods.

Thermal properties of interest for conductive heat transfer flame modeling consist of the thermal mass (ρc_p), thermal conductivity (k), ignition temperature of the energetic material regimes (T_{ig}), adiabatic flame temperature of energetic material chemistry

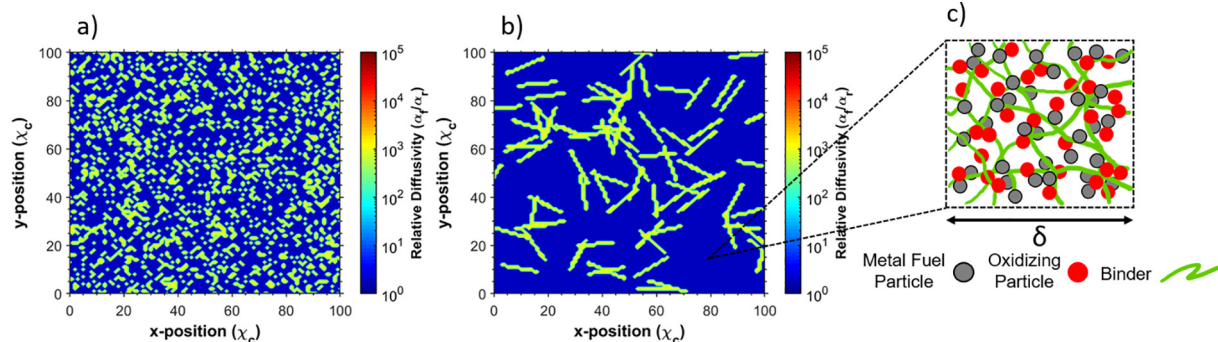


Fig. 2. Relative thermal diffusivity ($\frac{\alpha}{\alpha_0}$) mapping with respect to volume fraction for a) simple homogeneously mixed, uniform distribution, and b) distribution of rod of variable aspect ratios as well as an example of c) the heterogeneity scaling of solid energetic constituents relative to δ .

(T_{ad}), and characteristic time of reaction (τ_{rxn}). Given that the thermal mass for constituents of potential interest (e.g. Al, Ti, Cu, C, PVDF, Viton) have the same order of magnitude, the thermal mass of each material type throughout this analysis remains invariant at a value of $10^6 \text{ J m}^{-3} \text{ K}^{-1}$. The quantitative value of thermal conductivity of the energetic material has a lower bound based on the binder. Neat polymer binders such as Viton and PVDF have thermal conductivities of $\sim 0.2 \text{ W m}^{-1} \text{ K}^{-1}$ which increase with the addition of thermally conductive fuels (Du et al., 2018; Zhou et al., 2012; Bama et al., 2009; Wang et al., 2019). For simplicity, the energetic material possesses a thermal conductivity, k_o , of $0.4 \text{ W m}^{-1} \text{ K}^{-1}$ (double PVDF) (Zhou et al., 2012) with the inert rods having varied thermal conductivities higher than the energetic material. The chosen ignition temperature and adiabatic flame temperature are based on Al/CuO thermite composites which have a measured ignition temperature of $\sim 900 \text{ K}$, and a theoretical adiabatic flame temperature of $\sim 2800 \text{ K}$ (Rehwoldt et al., 2020; Wang et al., 2019). The rough order of magnitude of the time of reaction is based on quasi-homogenous flame propagation (Lahiner et al., 2017) and laminar flame theory (Goroshin et al., 1998) with experimental observations of Al/CuO propellants which satisfy the assumption of fast chemistry (Wang et al., 2019; Lahiner et al., 2017).

3. Results

3.1. Role of rod aspect ratio in combustion performance

Flame propagation modeling was carried out over a $500 \mu\text{s}$ time period. Energetic composites are incorporated with randomly oriented rods at varied volume percentages (vol% = 0%, 5%, 10%, 20%, 30%, 40%) and aspect ratios (AR = 1, 5, 15, 25, 35, 45, 55). Modeling of each parameter set was repeated 5 times. Temperature mappings in Fig. S3 illustrate overall flame morphology with hot spots designating zones undergoing transient exothermic chemistry. Analysis of flame propagation focuses on how the integration of thermally conductive rods ($k = k_o \times 10^4$) may assist proliferation of energy throughout the composites and enhance the amount of energy released within the combustion time interval. The energy release of the system may be expressed by Equation (4) which can be simplified to a dimensionless energy in Equation (5). The dimensionless energy release is defined as the relative change in the energy release of the composite compared to the case without rods.

$$\frac{\Delta E}{\Delta t} \approx \rho c_p \Delta T \frac{\Delta V}{\Delta t} = \rho c_p \delta (T_{ad} - T_{ig}) \frac{A_E}{\tau_{total}} \quad (4)$$

$$\frac{\left(\frac{\Delta E}{\Delta t}\right) - \left(\frac{\Delta E}{\Delta t}\right)_o}{\left(\frac{\Delta E}{\Delta t}\right)_o} = \frac{\rho c_p \delta (T_{ad} - T_{ig}) \frac{A_E}{\tau_{total}}}{\rho c_p \delta (T_{ad} - T_{ig}) \frac{A_o}{\tau_{total}}} - 1 = \frac{A_E}{A_o} - 1 \quad (5)$$

The energy release of the composite is directly related to the cross-sectional burned area, A_E , of energetic material assuming that the propagation behavior is relatively invariant along the thickness of the composite. The rods are incorporated to enhance pre-heating of material ahead of the main flame front. As such, analysis of flame propagation is assessed based on the degree of pre-heating, total area burned, and energetic material burned after the primary ignition transient. The pre-heated zone and total area burned are defined as the accumulation of temperature nodes which exceed 500 K and the ignition temperature (900 K), respectively. Given that the rods are non-energetic, the area of burned energetic material is simply a subset of the total area burned. An illustration is shown in Fig. 3a outlines each area type of interest with the distribution of rods superimposed.

As suggested, the pre-heated area is always larger than the accumulated total area burned and the burned energetic material area. One can see from the snapshot of the pre-heated zone in Fig. 3a that the heat preferentially flows along the direction of the rods, ahead of the outlined total area burned ($T > T_{ign}$). The time-resolved graph in Fig. 3b depicts sudden jumps in the pre-heated area which corresponds to sudden increases in material conductivity due to local packing of the rods. These sudden changes are mirrored by the total area burned after a lag time corresponding to the time necessary for heat to diffuse outward from the rods to initiate chemistry.

3.1.1. Flame propagation and energy release rates

Dimensionless comparisons of combustion performance between systems of various aspect ratios and volume percentages of rods are made in Fig. 4 by plotting the percentage change in the total area burned, $\frac{A_{total}}{A_o} - 1$, and energy released relative to a composite with no rods added. Additionally, the ratio of accumulated pre-heated area relative to the total area burned is calculated to quantify how the role of pre-heating correlates to propagation behavior.

The total area burned acts as surrogate for the flame propagation rate (Fig. 4a) where it can be seen that the total area burned is enhanced by up to 25% for most rod aspect ratios up to $\sim 30 \text{ vol}\%$. Interestingly, the region of maximum enhancement between 10 and 30 vol% appears to correlate to the range of volume percentages for which previous studies using carbon-based fillers (e.g. graphite, carbon nanotubes, carbon fibers) have experimentally observed the much-debated thermal percolation behavior (Kargar et al., 2018; Smith et al., 2017; Meeks et al., 2017; Zheng et al., 2012). However, further increases to the vol% of added rods results in a steep regression in total area burned as a result of reduced vol% of energetic material (Supplemental Video). Increasing the aspect ratio of rods appears to enhance the total area

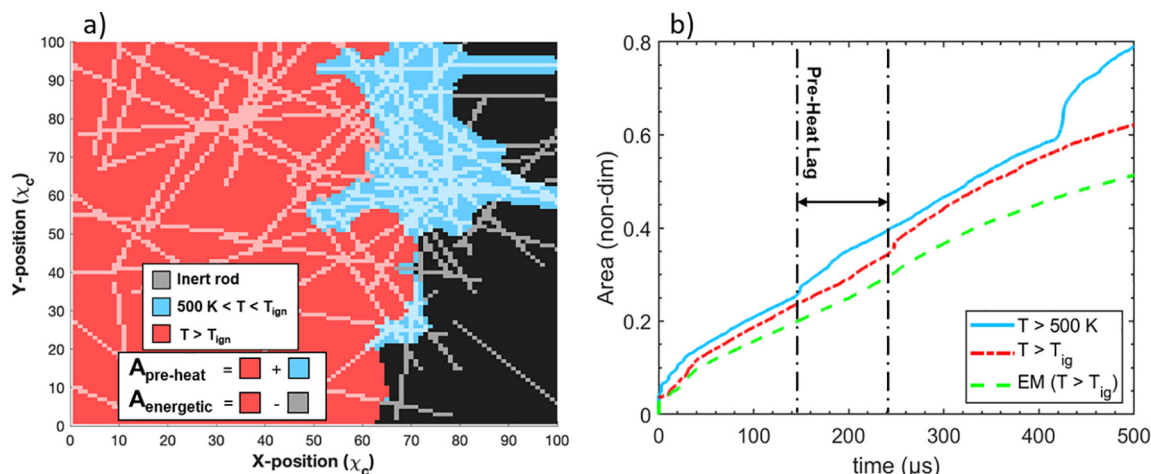


Fig. 3. a) Flame front snapshot and b) time resolved behavior of the accumulated area of the pre-heated zone, total burned material, and burned energetic material for the case of AR = 55, vol%=20, $t = 480\ \mu\text{s}$ (left to right propagation).

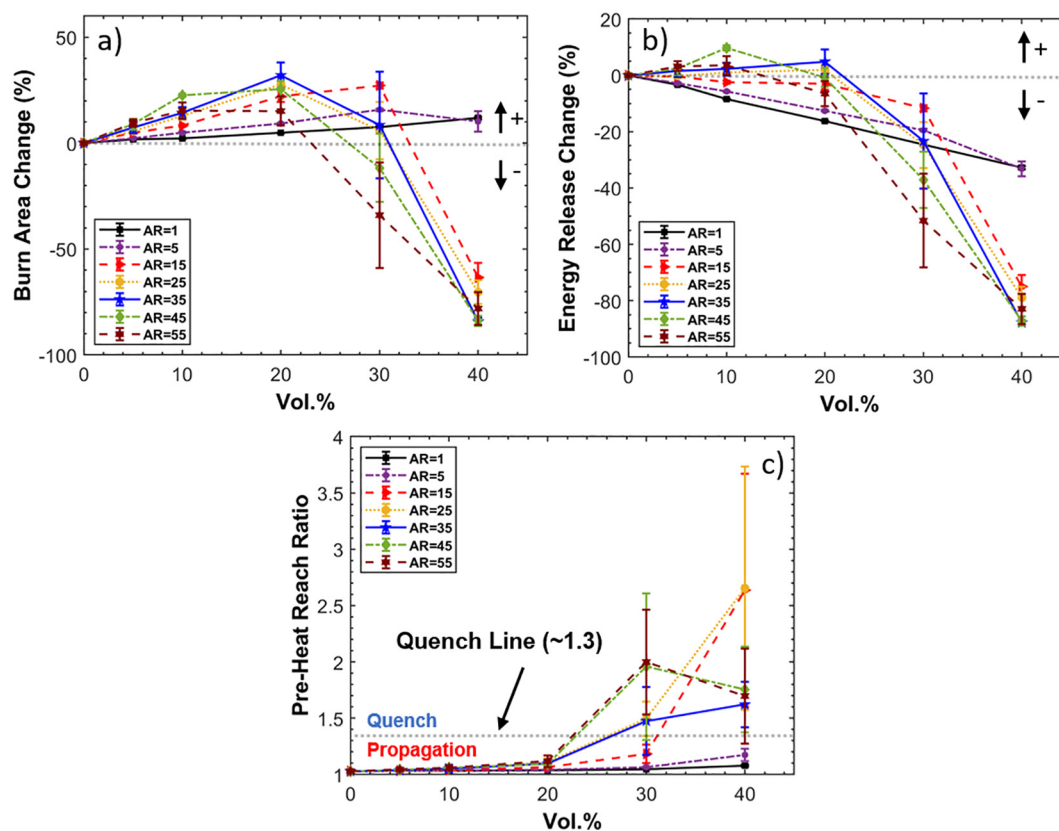


Fig. 4. Effect of aspect ratio and vol% of rods with a fixed thermal conductivity on a) the change in total area burned, b) energy released over the allotted burn time, and c) the extent of pre-heating during flame propagation.

burned and results in the onset of regressive behavior at lower vol% due to further isolation of energetic material regions.

The energy release of the system in Fig. 4b mirrors that of Fig. 4a in terms of the general behavior with respect to vol%. However, the energy released has a maximum enhancement of $\sim 10\%$ and a clear shift in the vol% region which constitutes a positive enhancement. The 20 vol% threshold marks the point in most of the ARs studied where replacing energetic material with thermally conductivity material is no longer beneficial for energy release. The addition of thermally conductivity materials is also not guaranteed to be beneficial with the lower half of ARs tested ($AR < 25$) resulting in

either negligible enhancements or reductions in energy release for vol% = 5, 10.

It appears that positive energy enhancement occurs for larger ARs and a range of low volume percentages (~ 5 – 10 vol%). There also seems to be a threshold where increases in AR no longer increase energy release rates. In Fig. 4a-b, the trend of increasing aspect ratio with increased energy release and total area burned regresses once the aspect ratio is increased to AR = 55. When evaluating even larger aspect ratio fillers, it becomes clear that the specific orientation of the rods becomes more important at lower vol% since the likelihood of the rods pointing in a direction

conductive for flame propagation diminishes. This behavior manifests itself in both the diminished enhancement to the total area burned and energy release as well as the standard error. As a result, there must exist a unique domain of volume percentages and aspect ratios for which the energy release rate and propagation rate are maximized for different energetic systems with randomly oriented rods of a specific thermal conductivity.

Combustion experiments studying directly biased thermally conductive pathways in energetic materials are limited in scope, but have shown to significantly enhance the effective thermal conductivity in two-phase systems (Agarwal et al., 2008; Isert et al., 2017). Modeling flame propagation using directionally manipulated rods is reserved for future works.

3.1.2. Pre-Heating of the flame front

The largest magnitude in the standard error for quantified values occurs at 30 vol% in Fig. 4a-b. This large error indicates a “do or die” region where there is nearly equal probability for flame propagation to either proceed or to quench. This behavior is linked to the competition between pre-heating which assists propagation and pre-heating which leeches the heat needed to sustain self-propagation. The precise behavior of pre-heating is likely dependent on specific thermochemical properties, but the values of the ratio of the pre-heated area ($T > 500$ K) to the total area burned ($T > T_{ig}$) can offer insight.

The representative pre-heat ratio for a single propagation run is determined by calculating the ratio at each time step and averaging the values over the last two-thirds of the total time steps. This is done to neglect the transient behavior of the initial heating process and effects due to propagation which nears the boundary of the material (Fig. S4). Fig. 4c shows the reach of pre-heating increases as the vol% increases for vol% up to 30%. Additionally, both the values of the pre-heat ratio and the corresponding standard error at 30 vol% clearly increases at higher aspect ratios. Increases in standard error and the pre-heat ratio express competing trends in which increases in aspect ratios may lead to propagation rate enhancements, but also may lead to increased likelihood of quenching. This trend breaks down at 40 vol% since it is nearly assured that higher aspect ratios will quench before establishing a self-propagating flame front.

One may roughly define a “quench line” as a threshold pre-heat value for which the probability of propagation quenching meets or exceeds the probability of sustained flame propagation. The exact position of this line is not precise but can be estimated based on the sensitivity of the standard error with respect to the collective aspect ratios as the pre-heat ratio value increases. This pre-heat ratio value of the quench line was found to be ~ 1.3 and corresponds to an accumulated pre-heat area which is roughly 30% larger than the accumulated total area burned.

3.2. Role of rod thermal conductivity in flame propagation

Inert rods are integrated into the energetic material to take advantage of their thermally conductive properties. We analyzed the role of the thermal conductivity of rods with a constant aspect ratio ($AR = 45$) on the total area burned and energy released over the total combustion time. Each volume percentage (vol% = 5, 10, 20) uses the same material mapping with varied rod thermal conductivity in order to focus on how the thermal conductivity, specifically, effects the total area burned and energy released. Fig. 5 shows how the combustion behavior changes at different volume percentages as the thermal conductivity of the rods is varied by 5 orders of magnitude relative to the energetic material ($\frac{k}{k_0} = 1, 10, 10^2, 10^3, 10^4, 10^5$). An example of the flame behavior with var-

ied rod thermal conductivity at 20 vol% is rendered in the thermal mappings displayed in Fig. 6.

We once again observe that, while the total area burned is maximized for 20 vol% rods, the energy release is maximized for 10 vol% of rods. The extent of pre-heating is greatest at higher volume percentage and higher thermal conductivity. The standard error of the pre-heat ratio is calculated with respect to its fluctuations as a function of time (Fig. S4) and is shown to increase with higher rod thermal conductivity. Although none of the parameters chosen resulted in quenching of the flame front, it can be inferred that higher thermal conductivity would result in an increased probability of quenching at higher vol%. What is most interesting, however, is that all calculated values in Fig. 5 reach a point where their behavior becomes effectively independent of the thermal conductivity of the filler. With our chosen parameters, this thermal conductivity threshold occurs around $\frac{k}{k_0} = 10^3$. The thermal mapping of the flame front in Fig. 6 illustrates how little total area burned is gained between 10^2 and 10^5 . With this in mind, the search for sophisticated materials with exceeding large thermal conductivities may appear moot for this application.

The thermal conductivity-independent regime may manifest as a result of the effective thermal conductivity at boundaries between nodes with different materials. As mentioned in Section 2, the effective thermal conductivity is calculated based on the equivalent thermal resistance to heat flow across a boundary of discrete material domains (Equation (2)) (Pietrak and Wiśniewski, 2015). While the effective thermal conductivity across the boundary for adjacent similar materials is equal to the bulk thermal conductivity, the effective thermal conductivity across boundaries of dissimilar materials can potentially be several orders of magnitude smaller. When the additive thermal conductivity is much larger than the thermal conductivity of the energetic material ($k \gg k_0$), it becomes clear that there is an asymptotic behavior of the amount of heat which is able to flow across the boundary as rod thermal conductivity increases. The limiting step of flame propagation becomes reliant on the thermal conductivity of the energetic material itself.

4. Conclusion

In this study, a 2D finite element model is employed to evaluate the role of thermally conductive, high aspect ratio additives on propagation behavior in condensed phase energetic composites. Increases in the total area burned and energy released was observed when the connectivity of thermally conductive rods throughout the composites is optimized at minimal volume percentages ($AR > 25, \text{vol\%} < 20$). In cases where the aspect ratio was too low ($AR < 25$) or additive vol% was too high (> 20 vol%), the additive either offered no enhancement due to heat transfer limitations or quenched flame propagation through excessive heat transfer to non-energetic regions. Enhancements were reduced at aspect ratios which were too high, inferring the increased importance for rod orientation. Independently varied rod thermal conductivity for the same additive distribution led to increased enhancements in total area burned and energy release up to some critical thermal conductivity where enhancements to flame propagation performance no longer depended on the thermal conductivity of the additive. Such behavior appears to originate from limitations in heat transfer introduced by boundary resistances between material types. This study serves as proof-of-concept for a method to enhance energy release by increasing heat transfer with additives in a manner that could be readily incorporated into the energetic composite manufacturing process.

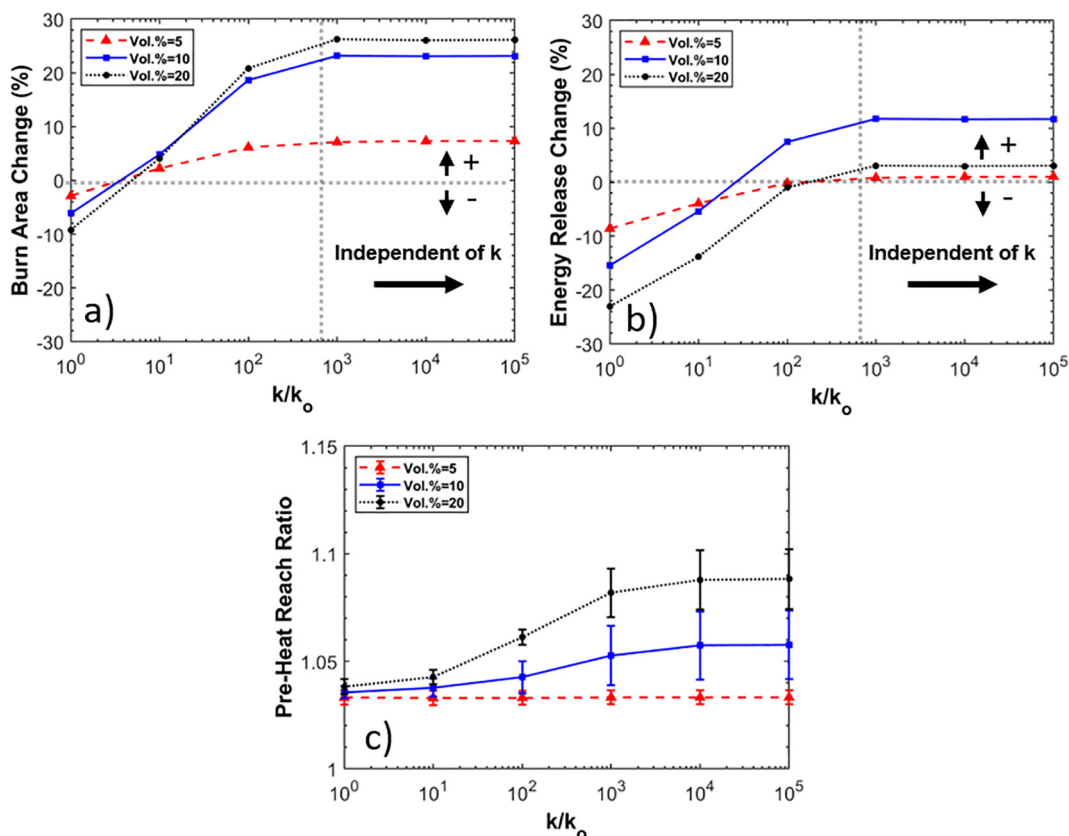


Fig. 5. Effect of thermal conductivity and vol% of rods with an aspect ratio (AR = 45) on a) the change in total area burned, b) energy released over the allotted burn time, and c) the extent of pre-heating during flame propagation.

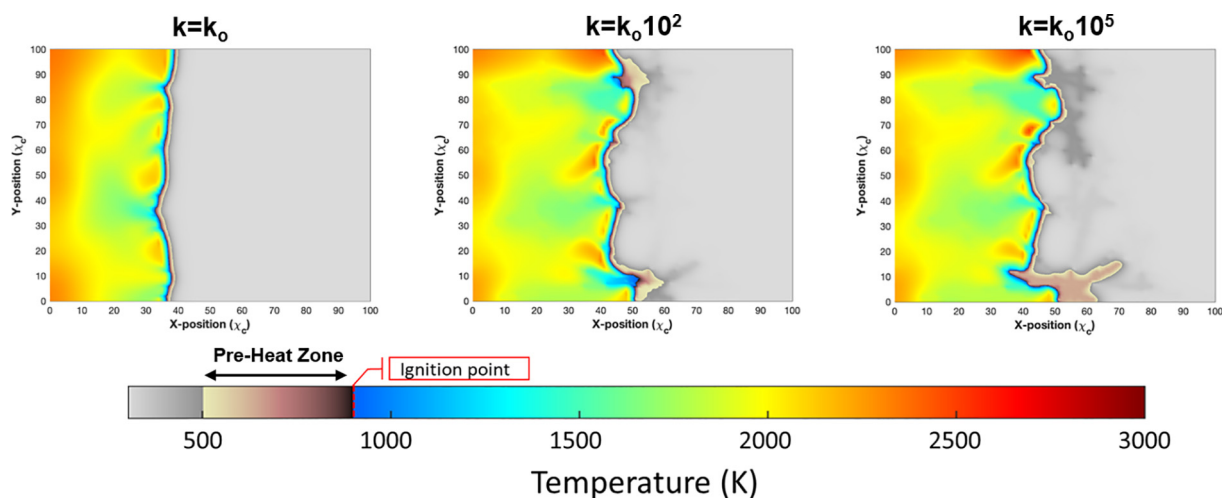


Fig. 6. Thermal mapping of energetic material propagation integrating rods with varied thermal conductivities within an invariant AR = 45 rod mapping of 20 vol% at $t = 325 \mu\text{s}$ (Propagation from left to right).

CRedit authorship contribution statement

Miles Rehwoldt: Conceptualization, Investigation, Methodology, Data Curation, Formal Analysis, Software, Visualization, Writing-original draft, Writing-review and editing. **Dylan Kline:** Conceptualization, Data Curation, Investigation, Formal Analysis, Software, Visualization, Writing-review and editing. **Michael Zachariah:** Conceptualization, Methodology, Project administration, Supervision, Funding acquisition, Validation, Writing-review & editing.

Declaration of Competing Interest

The authors declare that they have no known competing financial interests or personal relationships that could have appeared to influence the work reported in this paper.

Acknowledgments

This work was partially supported by the AFOSR.

Appendix A. Supplementary material

Supplementary data to this article can be found online at <https://doi.org/10.1016/j.ces.2020.116087>.

References

- Agarwal, S., Khan, M.M.K., Gupta, R.K., 2008. Thermal conductivity of polymer nanocomposites made with carbon nanofibers. *Polym. Eng. Sci.* 48, 2475–2481.
- An, T., Qu, W., Yang, Y., Zhao, F., Yan, Q., 2019. Preparation, characterization, and application of superthermites in solid propellants. Elsevier Inc.; 2019. <https://doi.org/10.1016/B978-0-12-813908-0.00004-6>.
- Bacciochini, A., Radulescu, M.I., Yandouzi, M., Maines, G., Lee, J.J., Jodoin, B., 2013. Reactive structural materials consolidated by cold spray: Al-CuO thermite. *Surf. Coatings Technol.* 226, 60–67. <https://doi.org/10.1016/j.surfcoat.2013.03.036>.
- Bama, G.K., Devi, P.I., Ramachandran, K., 2009. Structural and thermal properties of PVDF/PVA blends. *J. Mater. Res.* 44, 1302–1307. <https://doi.org/10.1007/s10853-009-3271-8>.
- Beck, J.M., Volpert, V.A., 2003. Nonlinear dynamics in a simple model of solid flame microstructure. *Phys. D Nonlinear Phenom.* 182, 86–102. [https://doi.org/10.1016/S0167-2789\(03\)00119-2](https://doi.org/10.1016/S0167-2789(03)00119-2).
- Becker, Kaus, Two-dimensional heat equation with FD, in: *Numer. Model. Earth Syst.*, 2016; pp. 1–9.
- Chakraborty, N., Swaminathan, N., 2007. Influence of the Damköhler number on turbulence-scalar interaction in premixed flames. I. Physical insight. *Phys. Fluids* 19. <https://doi.org/10.1063/1.2714070> 045103.
- Chen, R., Luo, Y., Sun, J., Li, G., 2012. Preparation and properties of an AP/RDX/SiO₂ nanocomposite energetic material by the sol-gel method. *Propellants. Explos. Pyrotech.* 37, 422–426. <https://doi.org/10.1002/prep.201000151>.
- Cheng, S.C., Vachon, R.I., 1969. The prediction of the thermal conductivity of two and three phase solid heterogeneous mixtures. *Int. J. Heat Mass Transf.* 12, 249–264. [https://doi.org/10.1016/0017-9310\(69\)90009-X](https://doi.org/10.1016/0017-9310(69)90009-X).
- Dang, Z., Yuan, J., Yao, S., Liao, R., 2013. Flexible nanodielectric materials with high permittivity for power energy storage. *Adv. Mater.* 25, 6334–6365. <https://doi.org/10.1002/adma.201301752>.
- Du, C., Li, M., Cao, M., Feng, S., Guo, H., 2018. Enhanced thermal and mechanical properties of polyvinylidene fluoride composites with magnetic oriented carbon nanotube. *Carbon N. Y.* 126, 197–207.
- Ervin, V.J., Klett, J.W., Mundt, C.M., 1999. Estimation of the thermal conductivity of composites. *J. Mater. Sci.* 34, 3545–3553.
- Goroshin, S., Lee, J.H.S., Shoshin, Y., 1998. Effect of the discrete nature of heat sources on flame propagation in particulate suspensions. In: *Twenty-Seventh Symp. Combust. Combust. Inst.*, pp. 743–749.
- Grinchuk, P.S., 2013. Combustion of heterogeneous systems with a stochastic spatial structure near the propagation limits. *J. Eng. Phys. Thermophys.* 86, 875–887. <https://doi.org/10.1007/s10891-013-0907-y>.
- Huang, C., Jian, G., Delisio, J.B., Wang, H., Zachariah, M.R., 2014. Electro spray deposition of energetic polymer nanocomposites with high mass particle loadings: A prelude to 3D printing of rocket motors. *Adv. Eng. Mater.* 17, 95–101. <https://doi.org/10.1002/adem.201400151>.
- Hwang, S., Mukasyan, A.S., Varma, A., 1998. Mechanisms of combustion wave propagation in heterogeneous reaction systems. *Combust. Flame* 115, 354–363. [https://doi.org/10.1016/S0010-2180\(98\)00016-9](https://doi.org/10.1016/S0010-2180(98)00016-9).
- Iserl, S., Lane, C.D., Gunduz, I.E., Son, S.F., 2017. Tailoring burning rates using reactive wires in composite solid rocket propellants. *Proc. Combust. Inst.* 36, 2283–2290. <https://doi.org/10.1016/j.proci.2016.06.141>.
- Kargar, F., Barani, Z., Salgado, R., Debnath, B., Lewis, J.S., Aytan, E., Lake, R.K., Balandin, A.A., 2018. Thermal percolation threshold and thermal properties of composites with high loading of graphene and boron nitride fillers. *ACS Appl. Mater. Interfaces* 10, 37555–37565. <https://doi.org/10.1021/acsami.8b16616>.
- Kline, D.J., Alibay, Z., Rehwoldt, M.C., Idrogo-Lam, A., Hamilton, S.G., Biswas, P., Xu, F., Zachariah, M.R., 2020. Experimental observation of the heat transfer mechanisms that drive propagation in additively manufactured energetic materials. *Combust. Flame* 215, 417–424. <https://doi.org/10.1016/j.combustflame.2020.01.020>.
- Lahiner, G., Nicolle, A., Zapata, J., Marín, L., Richard, N., Rouhani, M.D., Rossi, C., Estève, A., 2017. A diffusion-reaction scheme for modeling ignition and self-propagating reactions in Al/CuO multilayered thin films. *J. Appl. Phys.* 122. <https://doi.org/10.1063/1.5000312> 155105.
- Lawless, Z.D., Hobbs, M.L., Kaneshige, M.J., 2020. Thermal conductivity of energetic materials. *J. Energ. Mater.* 38, 214–239. <https://doi.org/10.1080/07370652.2019.1679285>.
- Maiti, S.N., Ghosh, K., 1994. Thermal characteristics of silver powder-filled polypropylene composites. *J. Appl. Polym. Sci.* 52, 1091–1103. <https://doi.org/10.1002/app.1994.070520810>.
- McClain, M.S., Gunduz, I.E., Son, S.F., 2019. Additive manufacturing of ammonium perchlorate composite propellant with high solids loadings. *Proc. Combust. Inst.* 37, 3135–3142. <https://doi.org/10.1016/j.proci.2018.05.052>.
- Meeks, K., Smith, D.K., Clark, B., Pantoya, M.L., 2017. Percolation of a metallic binder in energy generating composites. *J. Mater. Chem. A* 5, 7200–7209. <https://doi.org/10.1039/c7ta00689f>.
- Merzhanov, A.G., 1969. The theory of stable homogeneous combustion of condensed substances. *Combust. Flame* 13, 143–156. [https://doi.org/10.1016/0010-2180\(69\)90045-5](https://doi.org/10.1016/0010-2180(69)90045-5).
- Mukasyan, A.S., Shuck, C.E., 2017. Kinetics of SHS reactions: A review. *Int. J. Self-Propagating High-Temperature Synth.* 26, 145–165. <https://doi.org/10.3103/S1061386217030049>.
- Mukasyan, A.S., Rogachev, A.S., Varma, A., 1999. Mechanisms of reaction wave propagation during combustion synthesis of advanced materials. *Chem. Eng. Sci.* 54, 3357–3367. [https://doi.org/10.1016/S0009-2509\(98\)00457-6](https://doi.org/10.1016/S0009-2509(98)00457-6).
- Mukasyan, A.S., Rogachev, A.S., 2008. Discrete reaction waves: Gasless combustion of solid powder mixtures. *Prog. Energy Combust. Sci.* 34, 377–416. <https://doi.org/10.1016/j.peccs.2007.09.002>.
- Muravyev, N.V., Monogarov, K.A., Schaller, U., Fomenkov, I.V., Pivkina, A.N., 2019. Progress in additive manufacturing of energetic materials: Creating the reactive microstructures with high potential of applications. *Propellants Explos. Pyrotech.* 44, 941–969. <https://doi.org/10.1002/prep.201900060>.
- Nielsen, L.E., 1974. The thermal and electrical conductivity of two-phase systems. *Ind. Eng. Chem. Fundam.* 13, 17–20. <https://doi.org/10.1021/i160049a004>.
- Niragire, L., 2013. 2D numerical heat inverse model for diffusivity coefficients in Cartesian coordinates.
- Oberlack, M., Arlitt, R., Peter, N., 2000. On stochastic Damkohler number variations in a homogeneous flow reactor. *Combust. Theory Model.* 4, 495–509. <https://doi.org/10.1088/1364-7830/4/4/307>.
- Pal, R., 2008. On the Lewis-Nielsen model for thermal/electrical conductivity of composites. *Compos. Part A Appl. Sci. Manuf.* 39, 718–726. <https://doi.org/10.1016/j.compositesa.2008.02.008>.
- Pietrak, K., Wiśniewski, T., 2015. A review of models for effective thermal conductivity of composite materials. *J. Power Technol.* 95, 14–24.
- Rehwoldt, M.C., Wang, H., Kline, D.J., Wu, T., Eckman, N., Wang, P., Agrawal, N.R., Zachariah, M.R., 2020. Ignition and combustion analysis of direct write fabricated aluminum/metal oxide/PVDF films. *Combust. Flame* 211, 260–269. <https://doi.org/10.1016/j.combustflame.2019.08.023>.
- Rogachev, A.S., 2003. Microheterogeneous mechanism of gasless combustion. *Combust. Explos. Shock Waves.* 39, 150–158. <https://doi.org/10.1023/A:1022956915794>.
- Rogachev, A.S., Baras, F., 2007. Models of SHS: An Overview. *Int. J. Self-Propagating High-Temperature Synth.* 16, 141–153. <https://doi.org/10.3103/s1061386207030077>.
- Shen, J., Wang, H., Kline, D.J., Yang, Y., Wang, X., Rehwoldt, M., Wu, T., Holdren, S., Zachariah, M.R., 2020. Combustion of 3D printed 90 wt% loading reinforced nanothermite. *Combust. Flame* 215, 86–92. <https://doi.org/10.1016/j.combustflame.2020.01.021>.
- Smith, D.K., Cano, J., Pantoya, M.L., 2017. Thermal and combustion properties of energetic thin films with carbon nanotubes. *J. Thermophys. Heat Transf.* 31, 1–5. <https://doi.org/10.2514/1.T5009>.
- Smolyakov, V.K., 2001. "Roughness" of the gasless combustion front. *Combust. Explos. Shock Waves.* 37, 274–284. <https://doi.org/10.1023/A:1017519821870>.
- Song, M.S., Ran, M.W., Kong, Y.Y., 2011. In situ fabrication of ZrC powder obtained by self-propagating high-temperature synthesis from Al-Zr-C elemental powders. *Int. J. Refract. Metal Hard Mater.* 29, 392–396. <https://doi.org/10.1016/j.ijrmhm.2011.01.013>.
- Tang, F.D., Higgins, A.J., Goroshin, S., 2009. Effect of discreteness on heterogeneous flames: Propagation limits in regular and random particle arrays. *Combust. Theory Model.* 13, 319–341. <https://doi.org/10.1080/13647830802632184>.
- Turns, S.R., 2012. *An introduction to Combustion Concepts and Applications*. McGraw-Hill.
- Varma, A., Mukasyan, A.S., Hwang, S., 2001. Dynamics of self-propagating reactions in heterogeneous media: Experiments and model. *Chem. Eng. Sci.* 56, 1459–1466. [https://doi.org/10.1016/S0009-2509\(00\)00371-7](https://doi.org/10.1016/S0009-2509(00)00371-7).
- Wanasinghe, D., Aslani, F., Ma, G., Habibi, D., 2020. Review of polymer composites with diverse nanofillers for electromagnetic interference shielding. *Nanomaterials* 10, 1–46.
- Wang, H., Delisio, J.B., Holdren, S., Wu, T., Yang, Y., Hu, J., Zachariah, M.R., 2018. Mesoporous silica spheres incorporated aluminum/poly(vinylidene fluoride) for enhanced burning propellants. *Adv. Eng. Mater.* 20, 1700547. <https://doi.org/10.1002/adem.201700547>.
- Wang, H., Rehwoldt, M., Kline, D.J., Wu, T., Wang, P., Zachariah, M.R., 2019. Comparison study of the ignition and combustion characteristics of directly-written Al/PVDF, Al/Viton and Al/THV composites. *Combust. Flame* 201, 181–186. <https://doi.org/10.1016/j.combustflame.2018.12.031>.
- Wang, H., Kline, D.J., Zachariah, M.R., 2019. In-operando high-speed microscopy and thermometry of reaction propagation and sintering in a nanocomposite. *Nat. Commun.* 10, 8. <https://doi.org/10.1038/s41467-019-10843-4>.
- Yan, S., Jian, G., Zachariah, M.R., 2012. Electrospun nanofiber-based thermite textiles and their reactive properties. *ACS Appl. Mater. Interfaces* 4, 6432–6435.
- Yuan, J., Yao, S., Li, W., Sylvestre, A., Bai, J., 2017. Anisotropic percolation of SiC-carbon nanotube hybrids: A new route toward thermally conductive high-k polymer composites. *J. Phys. Chem. C* 121, 12063–12070. <https://doi.org/10.1021/acs.jpcc.7b03372>.
- Zheng, R., Gao, J., Wang, J., Feng, S.P., Ohtani, H., Wang, J., Chen, G., 2012. Thermal percolation in stable graphite suspensions. *Nano Lett.* 12, 188–192. <https://doi.org/10.1021/nl203276y>.
- Zhou, W., Zuo, J., Ren, W., 2012. Thermal conductivity and dielectric properties of Al/PVDF composites. *Compos. Part A* 43, 658–664. <https://doi.org/10.1016/j.compositesa.2011.11.024>.